RSC Advances

PAPER

Published on 02 July 2026

Cite this: DOI: 10.1039/d6ra01504b

Mechanochemical synthesis of Ag nanoparticles using ascorbic acid

Ľudmila Balážová,[a] Adrian Augustyniak,[bc] Nina Daneu,[d] Tibor Sopčák,[e] Ivana Kočišová,[a] Imelda Octa Tampubolon[f] and Matej Baláž *[f]

Received 20th February 2026
Accepted 17th April 2026

DOI: 10.1039/d6ra01504b

rsc.li/rsc-advances

Mechanochemical synthesis of silver nanoparticles using ascorbic acid as a reductant was completed after 30 min of planetary ball milling, as confirmed by X-ray diffraction and FT-infrared spectroscopy. The estimated average crystallite size of the produced Ag nanoparticles was 54 ± 2 nm. TEM analysis revealed a polymodal distribution of Ag nanoparticles crystallite sizes. The product exhibited potent antibacterial activity against *E. coli* and *S. aureus*.

Mechanochemistry is a solvent-free, environmentally friendly pathway in line with green chemistry principles[1] and United Nations Sustainable Development Goals,[2] capable of yielding nanoparticles.[3] Contrary to the view of researchers outside the community that it is a top-down approach because it reduces particle size to the nanoscale, it also serves as a bottom-up approach by efficiently bringing precursors together at the nanoscale (or even beyond) where the reaction occurs. The individual units (atoms/molecules) grow to nanoparticles by the processes such as Ostwald ripening, oriented attachment, coalescence, atomic addition, *etc.*[4] Among many nanoparticle types, metallic silver nanoparticles (Ag NPs) are among the most studied[5] due to their great potential as antimicrobial agents.[6] A common synthesis pathway to reach Ag NPs involves the reduction of silver salts, most often silver nitrate. Common reducing agents encompass both organic and inorganic chemicals (*e.g.*, ascorbic acid (AA), hydroquinone, sodium borohydride or sodium citrate[7]). The selection of the reducing agent has an essential effect on the course of the reduction and the stability of Ag NPs.[8] Mechanochemical synthesis can be efficiently used to prepare Ag NPs.[4] The first report of the successful mechanochemical synthesis of Ag NPs by the reduction of AgCl by Na dates back to 2001.[9] Since then, the field has advanced significantly, and *in situ* monitoring techniques have been developed to track the progress of mechanochemical reactions, including the formation of Ag NPs during milling.[10] Besides synthetic chemicals, also natural biological materials can be used as reducing agents. This discovery enabled the formation of an expanding field of green synthesis of Ag NPs, utilising, *e.g.* plant extracts.[11,12] Mechanochemical approaches to produce Ag NPs *via* grinding silver salts and biological materials appeared quite recently.[13–19] However, working with biological materials always raises questions, which are mostly related to reproducibility issues due to the large number of species present in biological organisms. Therefore, we have decided to investigate the mechanochemical preparation of Ag NPs using a synthetic reducing agent in this work. Namely, AA was selected, as its lower reducing ability when producing metallic NPs *via* the mechanochemical synthesis observed so far poses a challenge. Recently, a combination of grinding and storage led to the successful synthesis of Ag NPs using AA within 2 days.[20] Interestingly, already in 2008, AA was used as an additive, to drive the mechanochemical reduction of AgCl by Cu to completion.[21] The present study is a first-ever report on a complete conversion of $AgNO_3$ to elemental Ag using ascorbic acid already during milling, without the need for subsequent storage.

The initial experiments were performed using zirconium oxide jars and balls, with a stoichiometric ratio of AA : $AgNO_3$ of 1 : 1, in line with the conditions used by De Oliveira *et al.*[22] to yield Au NPs. This amount of AA should be sufficient, as AA contains two carboxylic groups for the reduction of $AgNO_3$. The XRD patterns after 5 and 60 min of milling were very similar (see Fig. S1 in the SI). The diffractions of AA were absent already after 5 minutes, meaning a quick amorphization of its soft organic crystals. The diffractions of $AgNO_3$ (ICDD PDF2 card no. 01-074-2076) are present in both samples, albeit the intensities of certain diffractions are different. Whereas the intensities of the $AgNO_3$ diffractions in the milled samples are in accordance

[a]*Department of Pharmaceutical Technology, Pharmacognosy and Botany, The University of Veterinary Medicine and Pharmacy, Komenského 73, 041 81, Košice, Slovakia*

[b]*Department of Chemical and Process Engineering, Faculty of Chemical Technology and Engineering, West Pomeranian University of Technology in Szczecin, Al. Piastów 42, 71-065 Szczecin, Poland*

[c]*Center for Advanced Materials and Manufacturing Process Engineering (MATPRO), West Pomeranian University of Technology in Szczecin, Al. Piastów 42, 71-065 Szczecin, Poland*

[d]*Advanced Materials Department, Jožef Stefan Institute, Jamova Cesta 39, 1000 Ljubljana, Slovenia*

[e]*Institute of Materials Research, Slovak Academy of Sciences, Watsonova 47, 040 01 Košice, Slovakia*

[f]*Department of Mechanochemistry, Institute of Geotechnics, Slovak Academy of Sciences, Watsonova 45, 040 01, Košice, Slovakia*

with the database, the ones of the starting $AgNO_3$ do not correspond and exhibit preferred orientation, most probably due to imperfect sample preparation. The $AgNO_3$ diffractions in the milled powders are also slightly shifted to lower 2θ angles, either due to a smaller amount of powder available or because of the changes in the crystal lattice. These preliminary results show a minimal reaction progress. as the amount of formed elemental silver (ICDD PDF2 card no 00-004-0783) is tiny and does not change with time (its diffractions marked by an asterisk in Fig. S1). Thus, AA cannot effectively reduce silver nitrate under the given conditions, consistent with the mechanochemical synthesis of Au NPs.[23] To improve the reaction progress, further optimisation of experimental conditions was required.

Since there was still a large amount of non-reacted $AgNO_3$, it was hypothesised that potentially there is not enough AA present in the system, as *e.g.* in,[20] the process was the most efficient when the AA : $AgNO_3$ ratio was 3 : 1. The effect of AA over-stoichiometry was tested by using the AA : $AgNO_3$ molar ratios 3 : 1, 6 : 1 and 9 : 1 under identical milling conditions. The XRD patterns in Fig. S2 clearly show that increasing the AA amount does not improve the reaction progress. In fact, as the diffraction peaks corresponding to Ag^0 are barely visible when increasing the AA amount, the results are even worse than when using AA : $AgNO_3$ 1 : 1 stoichiometry.

Based on this observation, it was decided that, rather than changing the chemical factors, the energy supplied to the reaction mixture could be increased by using tungsten carbide jars and balls instead of zirconium oxide ones, and by increasing the number of milling balls. The energy supplied to the treated powders during high-energy milling can now be efficiently calculated applying the calculations given in.[24] The necessary input parameters encompass the following: effective diameter of the main disk of the planetary mill, diameter and height of the jar, diameter, mass and number of milling balls, rotation speed and milling time. In this way, the total energy (E_{total}) and impact energy (E_{impact}) can be calculated. The results of these calculations show that total energy transferred to the powder increased from 56.5 kJ (using 9 ZrO_2 milling balls with a diameter of 9.25 mm) to 395.6 kJ (using 25 WC milling balls with a diameter of 10 mm) during 45 minutes of milling. The XRD patterns in Fig. 1 clearly show a significant improvement in conversion compared with previous experiments, as the peaks of the starting $AgNO_3$ are already minor after a short milling time of 15 minutes. In contrast, those corresponding to Ag^0 are much more pronounced. In addition, a lower-intensity peaks belonging to neither precursors nor Ag^0 product were identified. These peaks were also observed in,[20] however, their presence was not discussed. Since they are crystalline even after intensive milling, their organic origin can be almost surely ruled out. More probably, they represent one of the following: (i) a silver – ascorbate salt/complex, or (ii) a mixed $AgNO_3$–AA co-crystal. For simplicity, this phase is referred to as an "intermediate" in the following text. Its four main diffractions are marked with an asterisk in Fig. 1 (for the sample treated for 30 min). Upon further processing, the diffractions corresponding to silver nitrate completely vanished from the XRD patterns. The XRD

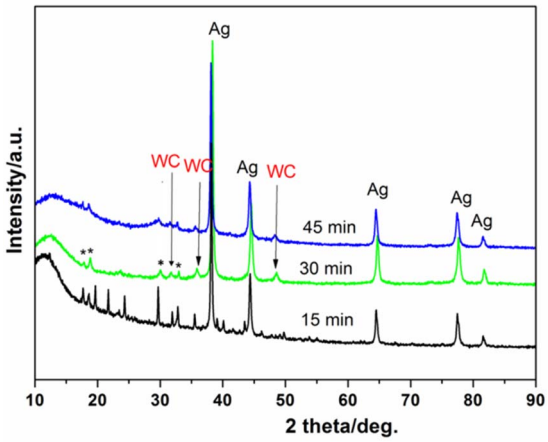

Fig. 1 XRD patterns of AA : $AgNO_3$ mixture with a 1 : 1 ratio using 10 mm WC balls after different milling times. The non-marked diffractions correspond to $AgNO_3$ (ICDD PDF2 card no 01-074-2076). Ag diffractions were assigned based on the ICDD PDF2 card no 00-004-0783. WC diffractions were assigned based on the ICDD PDF card no. 00-051-0939 asterisk marks an unidentified phase.

patterns obtained after 30 and 45 min of milling are almost identical, showing a significant reduction of diffractions corresponding to intermediate (*) and a slight contamination from WC milling media. Tungsten carbide contamination represents an inert material and its presence does not influence the conversion (this can be claimed as the reaction reached a significant conversion already after 15 min when WC presence was not proven). The reaction mixture after 45 min of milling became very sticky and difficult to handle. A similar phenomenon was observed during the solid-state synthesis of Ag NPs using PVP as reducing and stabilising agent.[13] In the mentioned study, prolonging reaction times from 15 min to 25–30 min caused the mixture to stick to the wall of the milling capsule. It was also shown that long milling times lead to a decrease in the surface area of NPs due to welding and coalescence.[25,26]

To mitigate WC contamination, the ball diameter was reduced to 5 mm. Namely, 177 pieces of 5 mm WC balls were used (this amount was used to keep the ball mass similar to the experiment with10 mm balls). However, no imprvement was achieved, as clearly higher WC content was evidenced (the XRD patterns of the mixtures after milling for 45 min using 5 and 10 mm balls are compared in Fig. S3). Moreover, the diffractions of the intermediate phase were more intensive when using 5 mm balls. The energy calculations showed that both the impact energy and the total energy supplied to the powders were higher when using 5 mm balls (E_{impact} = 37.2 J *vs.* 5.2 J, and E_{total} = 431.3 kJ *vs.* 395.6 kJ for the experiment using 177 pieces of 5 mm *vs.* 25 pieces of 10 mm balls, respectively). Thus, in this case, a mere change in the balls' diameter, while keeping the other parameters the same, did not result in reduced abrasion and seems to favor the intermediate stabilization.

Based on the above-described results, it was concluded that optimal conditions for the synthesis of elemental Ag were an AA : $AgNO_3$ ratio of 1 : 1, a milling time of 30 min, and the use of

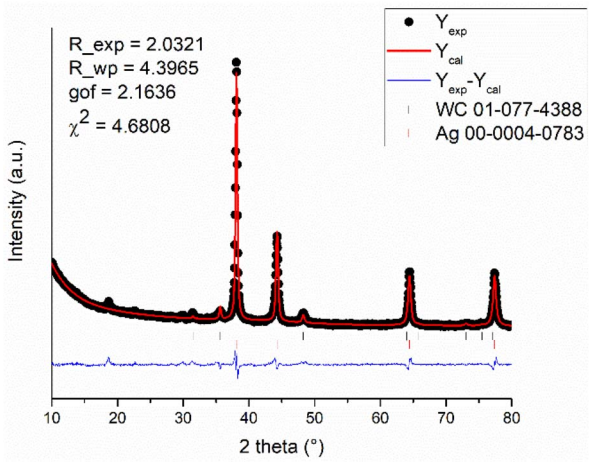

Fig. 2 XRD pattern of aged sample prepared for 30 min using 10 mm WC balls (Ag-AA-WC product) and Rietveld refinement results, including fitting factors.

10 mm WC balls. This accounts for the supplied total energy of 263.7 kJ.

To get more detailed information about the stability, phase content and crystallite size of the produced Ag NPs, the XRD pattern of the optimal sample was re-measured after 20 months using a different setup providing better signal-to-noise ratio and the obtained data were subjected to Rietveld refinement (Fig. 2). The major phase with the content of 93 ± 0.5% was elemental Ag^0, with WC abrasion as the only significant impurity. Traces of intermediate were also identified; however, the intensity of its diffraction peaks was very low (thus the aging promoted the conversion), so it was not considered during the refinement. The estimated crystallite size of the Ag NPs was 54 ± 2 nm, with a microstrain of 0.57 ± 0.13% contributing to peak broadening. The lattice parameter a in the cubic unit cell was equal to 4.08683 ± 0.00008 Å.

To further confirm the reaction completion, the FTIR spectra of the final product and starting materials were measured and are presented in Fig. 3. It can be clearly seen that the characteristic vibrations of the nitrate group originating from $AgNO_3$ at 1379 cm^{-1} (asymmetric stretching) and at 825 cm^{-1} and 731 cm^{-1} (bending) are absent in the IR spectrum of the as-prepared Ag-AA-WC product. As for ascorbic acid, the C=C bond stretching vibration at 1651 cm^{-1} and the C=O stretching vibration at 1755 cm^{-1} are also not observed in the product.[20] The successful oxidation of AA is also confirmed by the absence of the stretching vibration band corresponding to –OH group at 3535 cm^{-1} in the FTIR spectrum of Ag-AA-WC product. Also the stretching vibrations of dehydroascorbic acid, a reaction intermediate (that according to[20] should be present at around 1791 cm^{-1} and 1753 cm^{-1}) are absent, thus further confirming the reaction completion. This final aged sample was subjected to TEM analysis and antibacterial activity evaluation.

The morphological characteristics of the optimal sample obtained after 30 minutes of milling were studied with (scanning) transmission electron microscopy ((S)TEM). The analyses confirmed the successful synthesis of Ag NPs (Fig. 4), with particle sizes ranging from a few nm to about 100 nm. A low degree of agglomeration and an overall crystallite size lower

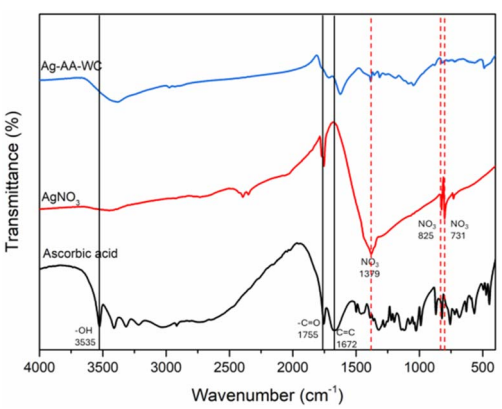

Fig. 3 FTIR analysis of precursors (ascorbic acid and $AgNO_3$) and Ag-AA-WC product.

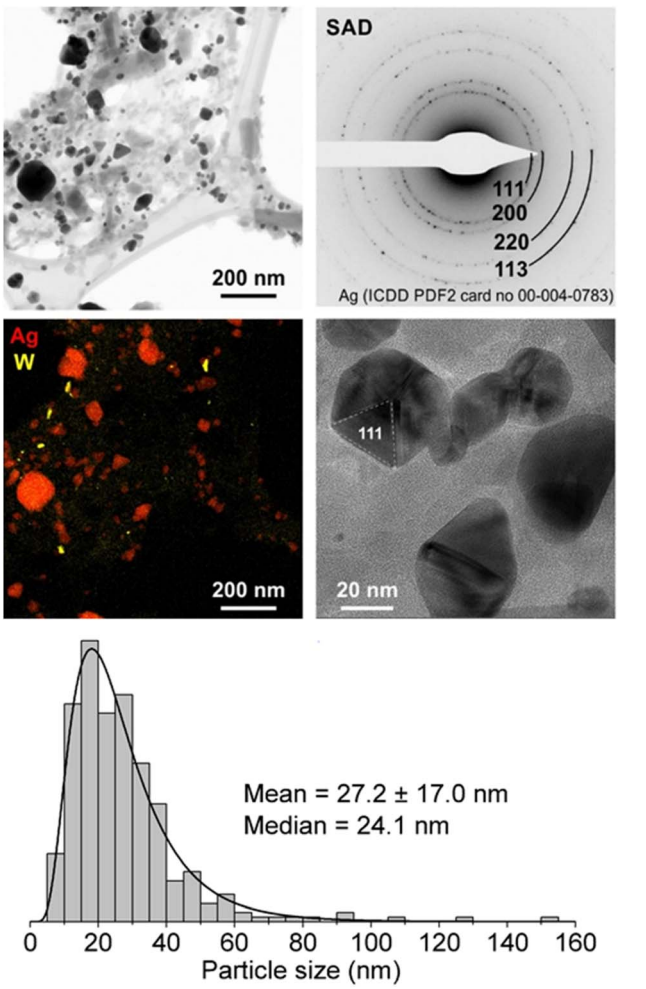

Fig. 4 TEM analysis of mechanochemically prepared Ag-AA-WC product: TEM image (top left), selected area diffraction (SAD) pattern (top right), elemental mapping showing Ag and W presence (middle left), high-resolution TEM image showing also (111) facet (middle right) and particle size histogram (bottom).

than that estimated from XRD data can be seen from Fig. S4–S7. The discrepancy of NPs crystallite size determination arises from the different nature of the two techniques. The estimated crystallite size obtained from Rietveld refinement of the XRD data reflects the average domain size of the whole sample and is based on statistically representative number of particles. In contrast, the TEM observations are based on a much smaller number of particles and may not be fully representative of the entire sample. In addition, the TEM grid preparation involves dispersing the powder in ethanol and depositing the suspended fraction onto the grid and thus, only the finer fraction of the sample is imaged. Selected area diffraction (SAD) pattern in Fig. 4 contained only diffraction rings with *d*-values of elemental silver with face-centred cubic structure. In contrast, the WC amount was too low to be detected by SAD. We used EDS mapping to reveal the presence of scarce WC nanoparticles among the prevalent Ag NPs. The smaller, isolated Ag NPs were mainly octahedral, enclosed by (111) facets. The detailed analysis of particle size (see histogram) showed wider unimodal size distribution of prepared Ag NPs. Namely, the sizes in the range 10–40 nm, with the average size of 27.2 ± 17.0 nm, were evidenced.

Further, the final product's antibacterial activity was evaluated and compared with that of the starting materials. The microbiological study confirmed that Ag-AA-WC sample (used at the concentration of 500 μg mL^{-1}) significantly reduced the viability of cells in the resazurin assay, regardless of the tested bacterium *Escherichia coli* and *Staphylococcus aureus* in the 4-hour acute toxicity test (Fig. 5). This effect is similar to that observed in previous studies on the same bacterial models that

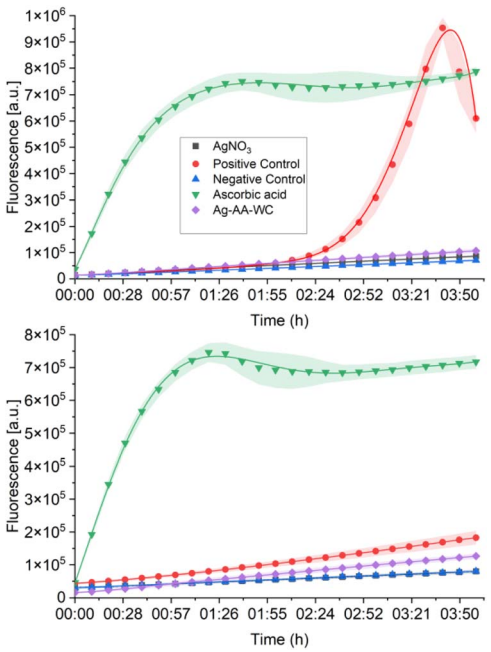

Fig. 5 Viability of *E. coli* (top) and *S. aureus* (bottom) bacteria in the control sample and the one contacted with the Ag-AA-WC sample and corresponding precursors. Positive control – bacterial cells only, negative control – assay with no cells.

Table 1 Comparison of selected facts of the studies focusing on mechanochemical synthesis of Ag nanoparticles utilizing ascorbic acid

Precursors	Mill type	Milling conditions	$AgNO_3$: AA molar ratio	Post-processing	Ag NPs crystallite size (nm)	Conversion after milling	$^aE_{total}$ (kJ)	$^aE_{impact}$ (mJ)	Reference
AgCl, Cu, AA	Planetary ball mill	700 rpm, 45 mL ZrO_2 jar; 7 pieces of 15 mm ZrO_2 balls; sample mass 4 g; 5 hours	Not stated, AA added in small amount as additive	Leached in 1.0 M NH_4OH and filtered	30–300 nm	Complete	561.1 kJ[b]	601.3 mJ[b]	21
$AgNO_3$, AA	Manual grinding (mortar and pestle)	30 min	1 : 1–1 : 8, 1 : 3 selected as ideal	Aged for 4, 8 and 24 h RT; washed, sonicated, centrifuged multiple times; dried at 60 °C for 24 h	Spherically shaped; 10.62 nm	Partial	—	—	20
$AgNO_3$, AA	Planetary ball mill	500 rpm; 80 mL WC jar; 25 pieces of 10 mm WC balls; sample mass 2 g; 30 min	1 : 1–1 : 9, 1 : 1 selected as ideal	None	54 ± 2 nm	Complete	263.7 kJ	5248.3 mJ	This study

[a] Calculated by utilizing tools described in (ref. 24). [b] Calculated using the estimations that the jar diameter and its height was the same as used in Pulverisette 7 premium line planetary ball mill (in ref. 21 Pulverisette 7 classic line was used), and also that the milling balls of ZrO_2 were not abraded.

were exposed to Ag^0/Ag_2CO_3-eggshell-plant nanocomposites.[27] The presence of fine WC particles as a result of contamination might also contribute to the antibacterial action.[28,29] Silver nitrate, used as a precursor to produce Ag-AA-WC, had a more substantial effect on bacterial populations than the tested product. This is well-visible in the zoomed in figures in the SI (Fig. S8 and S9). The fact that $AgNO_3$ shows stronger activity than the metallic Ag^0 is well-known from literature.[30,31] In our case, its better performance is caused by both the ionic character of silver in the solution and the fact that it is present in the liquid, where the diffusion is much faster than in solid state. However, the motivation to transform ionic form of silver into elemental one lies in the low stability of the former. AA interfered, as expected, with the resazurin assay, as it is a known interfering factor in this test.[32] However, the clearly distinct shape of the curve obtained for AA can serve as a suitable reference for comparisons. Namely, if AA would be present in our product, the corresponding curve would be bent up early in the process. As this is not the case, it may be concluded that the final product did not contain AA residues, or its amount was low enough not to interfere with the assay. It supports our finding that AA was oxidized during the synthesis of Ag NPs.

In the present contribution, we have shown a complete reduction of silver nitrate into elemental silver using ascorbic acid under mechanochemical solvent-free conditions. The comparison of selected information from the present study with that available for two other studies that used AA for similar purpose is shown in Table 1. It is clear that our approach offers the possibility to reach the desired product much faster. However, the higher sustainability value of the approach reported[20] has to be acknowledged. Upon combining the knowledge from the present contribution and the one reported therein, an even more green and sustainable protocol for producing Ag nanoparticles using ascorbic acid might be reached in the future.

Author contributions

Conceptualisation: ĽB, MBa, funding acquisition: MBa, investigation: ĽB, AA, ND, TS, IK, IOT, MBa, methodology: ĽB, MBa, ND, AA, project administration: MBa, resources: MBa, supervision: MBa, validation: ĽB, MBa, visualisation: ND, AA, TS, IOT, MBa, writing – original draft: ĽB, MBa, writing – review & editing: ĽB, MBa, ND, AA.

Conflicts of interest

There are no conflicts to declare.

Data availability

The experimental data regarding this article are available at https://zenodo.org/records/18399097.

Supplementary information (SI): the experimental conditions of the mechanochemical synthesis, characterization techniques (XRD and (S)TEM), antibacterial activity assessment, XRD patterns of the preliminary experiments, TEM images of the product and additional antibacterial activity plots. See DOI: https://doi.org/10.1039/d6ra01504b.

Acknowledgements

This work was supported by the Slovak Research and Development Agency under the contract No. APVV-24-0353. The support of the Slovak Grant Agency VEGA (grant 2/0039/26) is also gratefully acknowledged. The authors acknowledge fruitful discussions with Dr Martin Pisárčik and Dr Miloš Lukáč from the Faculty of Pharmacy, Comenius University, Bratislava, Slovakia, at the initial stage of experimental planning. The graphical abstract was prepared with the assistance of the AI tool ChatGPT (OpenAI).

Notes and references

1 K. Ardila-Fierro and J. Hernández, *ChemSusChem*, 2021, **14**, 2145–2162.
2 J. Alic, M. Schlegel, F. Emmerling and T. Stolar, *Angew. Chem., Int. Ed.*, 2024, **63**, e202414745.
3 P. Baláž, M. Achimovičová, M. Baláž, P. Billik, Z. Cherkezova-Zheleva, J. Criado, F. Delogu, E. Dutková, E. Gaffet, F. Gotor, R. Kumar, I. Mitov, T. Rojac, M. Senna, A. Streletskii and K. Wieczorek-Ciurowa, *Chem. Soc. Rev.*, 2013, **42**, 7571–7637.
4 P. F. M. De Oliveira, R. M. Torresi, F. Emmerling and P. H. C. Camargo, *J. Mater. Chem. A*, 2020, **8**, 16114–16141.
5 X. Zhang, Z. Liu, W. Shen and S. Gurunathan, *Int. J. Mol. Sci.*, 2016, **17**, 1534.
6 S. Ahmed, M. Ahmad, B. L. Swami and S. Ikram, *J. Adv. Res.*, 2016, **7**, 17–28.
7 I. Xavier, L. Lemos, E. de Melo, E. Campos, B. de Souza, L. Faustino, D. Galante and P. de Oliveira, *Phys. Chem. Chem. Phys.*, 2024, **26**, 11436–11444.
8 D. Veljovic, D. Guresic, A. Jokic, V. Vasic and B. Laban, *Chemistryselect*, 2020, **5**, 10488–10494.
9 J. Keskinen, P. Ruuskanen, M. Karttunen and S. Hannula, *Appl. Organomet. Chem.*, 2001, **15**, 393–395.
10 Y. Zheng, H. Kasai, S. Kobayashi, S. Kawaguchi and E. Nishibori, *Mater. Adv.*, 2023, **4**, 1005–1010.
11 A. Zuhrotun, D. Oktaviani and A. Hasanah, *Molecules*, 2023, **28**, 3240.
12 P. Singh, Y. J. Kim, D. Zhang and D. C. Yang, *Trends Biotechnol.*, 2016, **34**, 588–599.
13 D. Debnath, C. Kim, S. Kim and K. Geckeler, *Macromol. Rapid Commun.*, 2010, **31**, 549–553.
14 R. Arancon, A. Balu, A. Romero, M. Ojeda, M. Gomez, J. Blanco, J. Domingo and R. Luque, *Environ. Res.*, 2017, **154**, 204–211.
15 J. Kwiczak-Yigitbasi, M. Demir, R. Ahan, S. Canli, U. Seker and B. Baytekin, *ACS Sustainable Chem. Eng.*, 2020, **8**, 18879–18888.
16 M. Baláž, M. Goga, M. Hegedüs, N. Daneu, M. Kováčová, Ľ. Tkáčiková, Ľ. Balážová and M. Bačkor, *ACS Sustainable Chem. Eng.*, 2020, **8**, 13945–13955.
17 M. Baláž, Z. Bedlovičová, N. Daneu, P. Siksa, L. Sokoli, L. Tkáčiková, A. Salayová, R. Džunda, M. Kováčová,

R. Bureš and Z. Lukáčová-Bujňáková, *Nanomaterials*, 2021, **11**, 1139.
18 M. J. Rak, T. Friscic and A. Moores, *RSC Adv.*, 2016, **6**, 58365–58370.
19 M. Baláž, N. Daneu, Ľ. Balážová, E. Dutková, Ľ. Tkáčiková, J. Briančin, M. Vargová, M. Balážová, A. Zorkovská and P. Baláž, *Adv. Powder Technol.*, 2017, **28**, 3307–3312.
20 A. Zhang, Y. Tian, Y. Xiao, Y. Sun and F. Li, *Mater. Sci. Eng., B*, 2015, **197**, 5–9.
21 M. T. Le, D. J. Kim, C. G. Kim, J. S. Sohn and J. Lee, *J. Exp. Nanosci.*, 2008, **3**, 223–228.
22 P. de Oliveira, J. Quiroz, D. de Oliveira and P. Camargo, *Chem. Commun.*, 2019, **55**, 14267–14270.
23 P. de Oliveira, A. Michalchuk, J. Marquardt, T. Feiler, C. Prinz, R. Torresi, P. Camargo and F. Emmerling, *Crystengcomm*, 2020, **22**, 6261–6267.
24 O. F. Jafter, S. Lee, J. Park, C. Cabanetos and D. Lungerich, *Angew. Chem., Int. Ed.*, 2024, **63**, e202409731.
25 Y. Xia, Y. Xiong, B. Lim and S. E. Skrabalak, *Angew. Chem., Int. Ed.*, 2009, **48**, 60–103.
26 Y. Xia, X. Xia and H.-C. Peng, *J. Am. Chem. Soc.*, 2015, **137**, 7947–7966.
27 M. Baláž, M. Casas-Luna, A. Augustinyak, L. Tkáčiková, K. Szmuc, M. Kováčová, L. Čelko and Y. Shpotyuk, *Appl. Nanosci.*, 2022, **12**, 1899–1916.
28 F. O. Osazee, K. E. Mokobia and I. H. Ifijen, *Biomed. Mater. Devices*, 2024, **2**, 614–629.
29 C. Bankier, R. K. Matharu, Y. K. Cheong, G. G. Ren, E. Cloutman-Green and L. Ciric, *Sci. Rep.*, 2019, **9**, 16074.
30 C. Beer, R. Foldbjerg, Y. Hayashi, D. S. Sutherland and H. Autrup, *Toxicol. Lett.*, 2012, **208**, 286–292.
31 W. R. Li, T. L. Sun, S. L. Zhou, Y. K. Ma, Q. S. Shi, X. B. Xie and X. M. Huang, *Int. Biodeterior. Biodegrad.*, 2017, **123**, 304–310.
32 E. M. Czekanska, in *Mammalian Cell Viability: Methods and Protocols*, ed. M. J. Stoddart, 2011, vol. 740, pp. 27–32.